

Article

Infrared Image Enhancement Using Convolutional Neural Networks for Auto-Driving

Shunshun Zhong, Luwei Fu and Fan Zhang *

School of Automation, State Key Laboratory of Precision Manufacturing for Extreme Service Performance, Central South University, Changsha 410083, China; 18890095056@163.com (S.Z.); zf20072225@126.com (L.F.)

* Correspondence: zhangfan219@csu.edu.cn

Abstract: Auto-driving detection usually acquires low-light infrared images, which pose a great challenge to the autopilot function at night due to their low contrast and unclear texture details. As a precursor algorithm in the field of automatic driving, the infrared image contrast enhancement method is of great significance in accelerating the operation speed of automatic driving target recognition algorithms and improving the accuracy of object localization. In this study, a convolutional neural network model including feature extraction and image enhancement modules is proposed to enhance infrared images. Specifically, the feature extraction module consists of three branches, a concatenation layer, and a fusion layer that connect in parallel to extract the feature images. The image enhancement module contains eight convolutional layers, one connectivity layer, and one difference layer for enhancing contrast in infrared images. In order to overcome the problem of the lack of a large amount of training data and to improve the accuracy of the model, the brightness and sharpness of the infrared images are randomly transformed to expand the number of pictures in the training set and form more sample pairs. Unlike traditional enhancement methods, the proposed model directly learns the end-to-end mapping between low- and high-contrast images. Extensive experiments from qualitative and quantitative perspectives demonstrate that our method can achieve better clarity in a shorter time.

Keywords: infrared image enhancement; neural networks; pattern recognition; auto-driving



Citation: Zhong, S.; Fu, L.; Zhang, F. Infrared Image Enhancement Using Convolutional Neural Networks for Auto-Driving. *Appl. Sci.* **2023**, *13*, 12581. <https://doi.org/10.3390/app132312581>

Academic Editor: Yutaka Ishibashi

Received: 26 October 2023

Revised: 11 November 2023

Accepted: 13 November 2023

Published: 22 November 2023



Copyright: © 2023 by the authors. Licensee MDPI, Basel, Switzerland. This article is an open access article distributed under the terms and conditions of the Creative Commons Attribution (CC BY) license (<https://creativecommons.org/licenses/by/4.0/>).

1. Introduction

High-quality infrared images play a crucial role in scenarios such as auto-driving, fault diagnosis, and fire detection [1–4]. However, the quality of infrared images obtained in real-life scenarios tends to be poor due to environmental effects and the limitations of infrared thermal imaging technology [5]. The low contrast and unclear texture details of infrared images largely increase the difficulty of subsequent processing, such as detection, perception, and location [1,6–8]. Low-contrast infrared images lead to large deviations in target localization, so the first step in target localization is to increase the contrast of the image. Traditional infrared image enhancement methods are mainly divided into three types: histogram-based methods, transform function-based methods, and transform domain-based methods. Most of the traditional methods need to set parameters artificially, which enormously reduces the flexibility of applications [9]. Moreover, it takes a longer time to process larger-resolution images via traditional methods. Predicting the target and background precisely is crucial to achieve the aim of improving image contrast robustly. Unlike with fixed filters, we try to learn the filters suitable for extracting the target and background sub-images using a data-driven method. Inspired by the ability of convolutional neural networks (CNNs) in the image classification field, we propose a novel approach to predicting target and background features using filters learned by a CNN for infrared image enhancement.

In this paper, we propose a convolutional neural network model to enhance the quality of infrared images. The model consists of two parts: a feature extraction module and an

image enhancement module. We consider low-contrast infrared image enhancement as a supervised learning problem, and the model learns the end-to-end mapping between low- and high-contrast images, directly. Then, the targets and background clutters are predicted from the extracted multiscale feature images by the learned feature extraction module. Finally, the weak infrared image is enhanced by zooming in on the target while removing background clutter in the image enhancement module.

The contributions of our work can be summarized in three ways.

(1) Convolutional neural networks consisting of a feature extraction module and image enhancement module are applied to infrared image enhancement.

(2) The low- and high-contrast images are considered the input and output of the model for training. To overcome the lack of a large amount of training data, the brightness and clarity of the infrared images are randomly reduced to form sample pairs.

(3) Extensive experiments show that our method can not only effectively improve the quality of infrared images, but also reduce processing time.

2. Related work

2.1. Traditional Methods

Histogram equalization (HE) is one of the most common methods used to improve image contrast [10]. The main idea is to count the histogram of grayscale pixels in an image, and then, adjust the distribution characteristics of the grayscale pixels to improve the image contrast. This method treats each pixel point in the image individually without considering the relationship between its domains. To solve this problem, many scholars have proposed improved methods for HE. Liu et al. [11] proposed a two-dimensional HE algorithm that uses the contextual information around each pixel to enhance the image contrast. In addition, many scholars also transform the image from the spatial domain to the frequency domain via fast Fourier transform or wavelet transform, and process the relevant frequencies to adjust the image contrast. Singh et al. [12] combined lifting discrete wavelet transform and singular value decomposition for low-contrast image enhancement. Zhang et al. [13] conducted a gradient-domain-based visualization method for high-dynamic-range compression and detail enhancement of infrared images. Since then, researchers have proposed filtering framework algorithms based on this technique. Song et al. [14] proposed a detail enhancement algorithm for infrared images based on local edge-preserving filtering, which divides the image into base and detail layers. Then, the base layer and detail layer are processed separately to obtain the respective enhanced images, and finally, a better ratio is selected to fuse the enhanced images of the base and the detail layer components. As a result, it takes a long time to enhance images with a larger resolution using the filtering framework algorithm.

2.2. Deep Learning Method

Convolutional neural networks are widely used in areas such as image classification and target detection. In addition, researchers have also applied them to image enhancement [15–18]. Shen et al. [19] combined convolutional neural networks with retinex theory to propose MSR-net for low-light image enhancement. Kuang et al. [20] proposed a conditional generative adversarial network to address infrared image enhancement, which can avoid background noise being amplified and further enhance contrast and details. Cai et al. [21] proposed a trainable end-to-end system named DehazeNet, which takes a hazy image as input and outputs its medium transmission map, which is subsequently used to recover a haze-free image via an atmospheric scattering model. Qian et al. [22] proposed a neural network named a multi-scale error feedback network to enhance low-light images. Wang et al. [23] presented an innovative target attention deep neural network to achieve discriminative enhancement in an end-to-end manner. The above study illustrates that CNNs are useful for being able to enhance the contrast of infrared images.

3. Methodology

In this section, we use convolutional neural networks consisting of feature extraction and enhancement modules to enhance infrared images. The input image is first processed by the feature extraction module, and then, goes to the image enhancement module and finally outputs the enhanced image. The function of the feature extraction module is to extract the features of the input IR image and to concatenate and fuse these features to obtain a pre-fused image. The enhancement module is utilized to enhance the pre-fused image and to obtain a result similar to the target image. In the proposed method, infrared image enhancement is considered a supervised learning problem, and low- and high-contrast images are considered input and output data, respectively. Figure 1 shows the structure of our model.

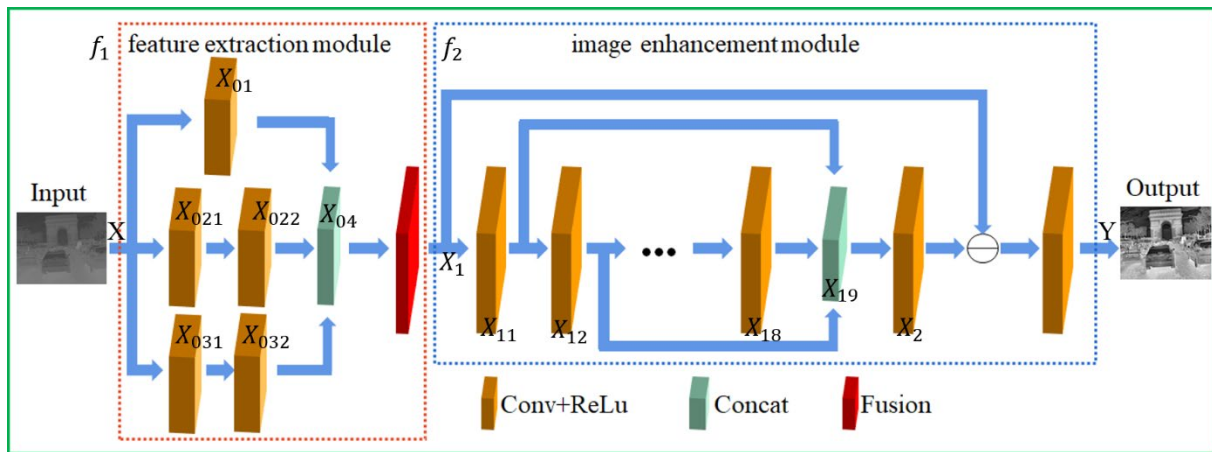


Figure 1. Structure of the proposed convolutional neural network for infrared image enhancement.

We define the low-contrast image as the input X , and the corresponding high-contrast image as the output Y . Assuming that f_1 and f_2 denote the function of the feature extraction and image enhancement modules, respectively, our model can be written as a combination of two functions:

$$Y = f(X) = f_2(f_1(X)) \tag{1}$$

The feature extraction module consists of three branches, a concatenation layer, and a fusion layer. The three branches are connected in parallel to extract the first, second, and third feature images from the input infrared image. The first branch includes a convolutional layer and a ReLU activation layer.

$$X_{01} = \max(0, X * W_{01} + b_{01}) \tag{2}$$

Here, X_{01} denotes the output of the first branch, and $*$ denotes the convolution operation. W_{01} and b_{01} denote the convolution kernel of the convolution layer and offset, respectively. \max corresponds to ReLU operation.

The second and third branches both include two convolutional layers and a ReLU activation layer:

$$X_{0i1} = \max(0, X * W_{0i1} + b_{0i1}) \tag{3}$$

$$X_{0i} = \max(0, X_{0i1} * W_{0i2} + b_{0i2}) \quad (i = 2, 3) \tag{4}$$

where X_{0i} denotes the output of the i branch, and X_{0i1} denotes the output of the first convolutional layer and ReLU activation layer of the first branch. W_{0i1} and b_{0i1} are the convolutional kernel and offset for the first convolutional layer in branch i , respectively. W_{0i2} and b_{0i2} are the convolutional kernel and offset for the second convolutional layer in branch i , respectively.

The concatenation layer connects the feature image outputs from the three branches by channel. The input of the fusion layer is the output of the concatenation layer, and outputs the pre-fusion image, including a convolutional layer and a ReLU activation layer.

$$X_{04} = [X_{01}, X_{02}, X_{03}] \quad (5)$$

$$X_1 = \max(0, X_{04} * W_{04} + b_{04}) \quad (6)$$

Here, X_{04} denotes the output of the splicing layer. W_{04} and b_{04} denote the convolution kernel of the convolution layer in the fusion layer and the offset, respectively.

The training images in the dataset usually have low luminance, so an image enhancement module is proposed following the convolutional difference strategy. The input of the image enhancement module is X_1 , which generates an output X_2 with the same width and height.

$$X_{11} = \max(0, X_1 * W_{11} + b_{11}) \quad (7)$$

$$X_{1i} = \max(0, X_{1(i-1)} * W_{1i} + b_{1i}) (i = 2, 3, \dots, 8) \quad (8)$$

Here, X_{11} denotes the output of the first convolution. W_{11} and b_{11} denote the convolution kernel and offset of the first convolution, respectively. W_{1i} and b_{1i} denote the convolution kernel and offset of the i convolution, respectively. The images after each convolution are then joined by the channel and convoluted again as follows:

$$X_{19} = [X_{11}, X_{12}, \dots, X_{18}] \quad (9)$$

$$X_2 = \max(0, X_{19} * W_{19} + b_{19}) \quad (10)$$

where X_{19} denotes the output after concatenation, and X_2 denotes the output after convolution. W_{19} and b_{19} denote the convolution kernel and offset, respectively. Finally, the final output image Y is obtained by convolving the difference between X_1 and X_2 :

$$Y = \max(0, (X_1 - X_2) * W_2 + b_2) \quad (11)$$

where W_2 and b_2 denote the convolution kernel and offset of the convolution, respectively. The sizes of the convolution kernels used in the convolution are 3 and 5.

4. Experiments

The experiments were conducted by using the deep learning framework TensorFlow 2.8.0 on a GPU RTX 2080Ti. Both the input and output image sizes were 200×200 . Before training the model, the input image was first transformed into a grayscale image, and then, normalized to input the model. Adam was used as the optimizer, and the learning rate was set to 0.0001. The batchsize and epoch were set to 8 and 50, respectively.

Let $\{X_i, Y_i\}_{i=1}^N$ be the training dataset, where X_i denotes the input infrared image, and Y_i denotes the corresponding output image. N is the number of training pairs. The infrared images used for training were derived from the FLIR thermal dataset, which contains a total of 14,000 8-bit images. FLIR is a thermal imaging dataset with a large number of low-contrast thermal imaging images, including mainly pedestrians and cars [24,25]. Complex image components and low contrast make it extremely difficult to recognize targets, hence the need for contrast enhancement of infrared images.

For the dataset of FLIR, similar images in the dataset were first removed and 6500 images were selected. Then, 500 images were randomly selected from these images to be flipped 45° , 90° , 135° , 180° , 225° , 270° , and 315° to enrich the training set and improve the quality of the model, which resulted in a total of 4000 images. The original 6000 images and the 4000 images obtained after flipping were treated as labeled images.

Finally, the contrast of the target image was reduced to obtain the training image. A training set containing 10,000 pairs was created, and 1000 images were selected from the dataset to form the test set.

The structural similarity index measure (SSIM) [26] and mean square error (MSE) [27] loss functions were used for the image enhancement class regression tasks. The SSIM is defined as follows:

$$SSIM(x, y) = \frac{(2\mu_x\mu_y + c_1)(2\delta_{xy} + c_2)}{(\mu_x^2 + \mu_y^2 + c_1)(\delta_x^2 + \delta_y^2 + c_2)} \tag{12}$$

where x is the original image, and y is the target image. μ_x and μ_y are the means of x and y , respectively. δ_x^2 and δ_y^2 are the variances of x and y . δ_{xy} is the covariances of x and y , respectively. c_1 and c_2 are constant to maintain stability, and are defined as follows:

$$c_1 = (k_1L)^2 \tag{13}$$

$$c_2 = (k_2L)^2 \tag{14}$$

where L is the dynamic range of the image, $k_1 = 0.01$, and $k_2 = 0.03$. The MSE is defined as

$$MSE(x, y) = \frac{1}{N} \sum_{i=1}^N (x_i - y_i)^2 \tag{15}$$

where x_i and y_i are the pixel points of x and y , respectively.

Figure 2 illustrates the loss changes with iteration number for MSE and SSIM. After two epochs, the loss values of the two types are reduced to 1/2 of that in the first epoch. After four epochs, the change in MSE loss is very small, but the change in SSIM loss is larger. Therefore, in terms of convergence speed, the MSE loss can reach stability in fewer epochs during training.

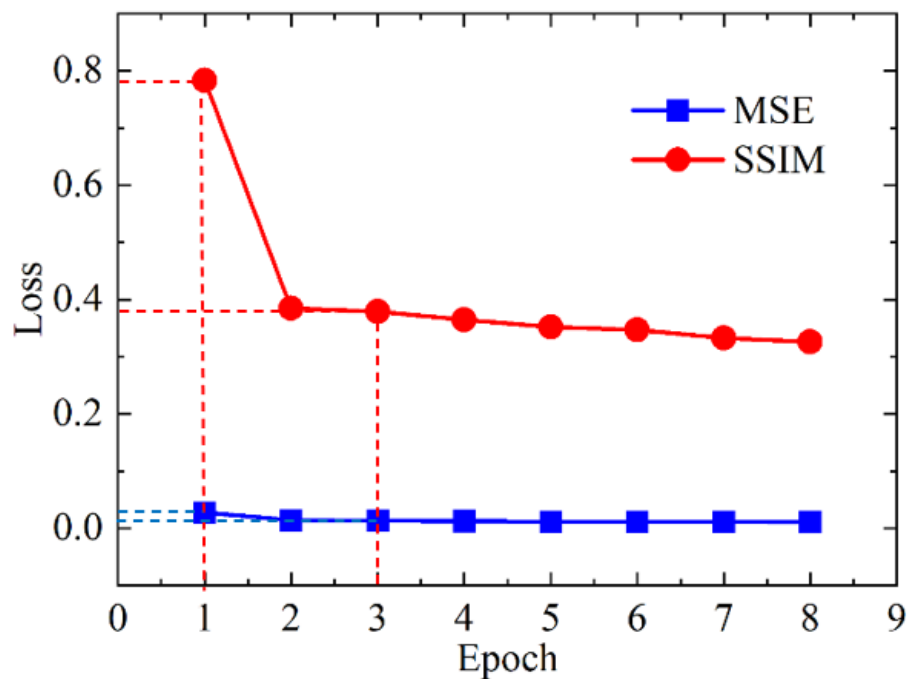


Figure 2. MSE and SSIM loss functions.

5. Results and Discussion

Figure 3 shows the input images, target images, and predicted images obtained using our proposed method. The target images and the predicted images are close in detail and contrast, and their subjective visual effects are similar. Table 1 shows the evaluation metrics, including contrast per pixel (CPP) [28], mean pixel contrast (MPC) [29], enhancement measure evaluation (EME) [30], image clarity (IC) [31], and entropy (E) [28]. Their formulas have the following representation:

$$CPP = \frac{1}{(H - 1)(W - 1)} \sum_x \sum_y \frac{|G(x, y)|}{\sqrt{2}} \tag{16}$$

$$MPC = \frac{C_{processed}}{C_{Original}} \tag{17}$$

$$EME_{\alpha, x, y}(\phi) = \frac{1}{xy} \sum_{l=1}^y \sum_{k=1}^y 20 \ln \frac{I_{max; k, l}^w(\phi \cdot par)}{I_{min; k, l}^w(\phi \cdot par) + c} \tag{18}$$

$$IC = \sigma_{RGYB} + (0.3\mu_{RGYB}) \tag{19}$$

$$E = - \sum_{i=0}^{l-1} P(q) \cdot \log(P(q)) \tag{20}$$

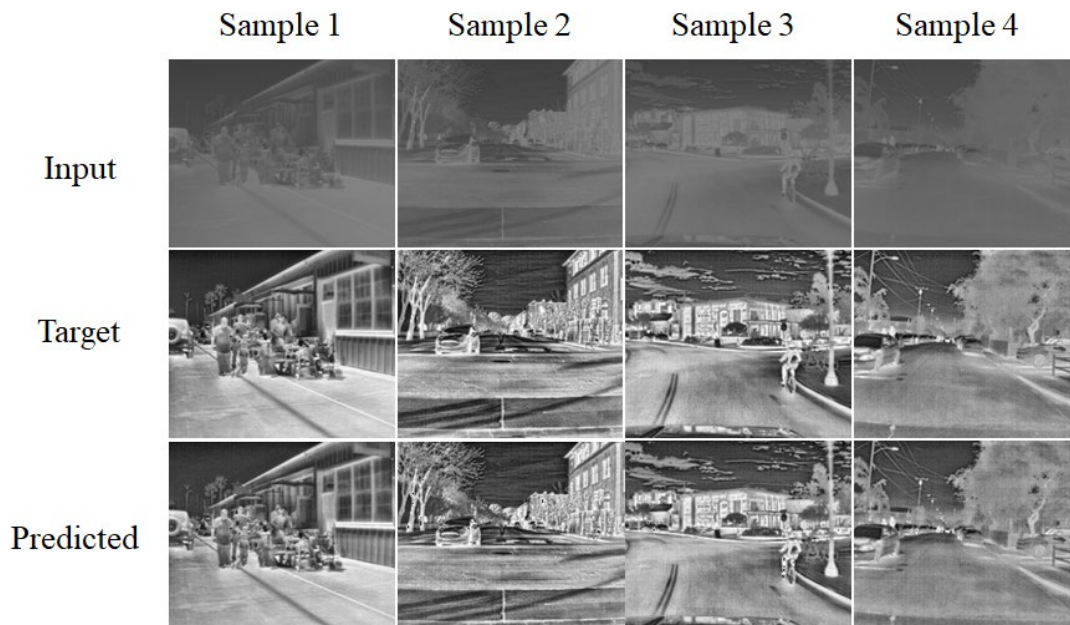


Figure 3. Input images, target images, and predicted images for road scenes.

In Equation (1), H and W represent the size of the image, and $G(x, y)$ is the gradient vector of the image. In Equation (2), C is the average contrast. $C_{processed}$ and $C_{Original}$ are the contrast of the input image and the processed image, respectively. For Equation (3), the image is broken up into x, y blocks, ϕ is the given transform, and α is an enhancement parameter. c is a constant value of 0.0001. In Equation (4), σ represents the standard deviation and μ is the mean value of all pixels. In Equation (5), E represents the set of image pixel values, q is the pixel of the image, and $P(q)$ represents the probability that one pixel value will appear.

For the first input image, the predicted results and the target image only differ significantly in the EME evaluation index, and are close in other aspects. For the second and third input images, there are large differences between the predicted and target images on EME

and CPP, and all other aspects are close. For the fourth input image, the predicted result and the target image only have a large difference on CPP, and the other aspects are close to each other. The results show that the predicted results are very close to the target images in terms of details. However, there is still room for improvement in our approach to EME and CPP.

Table 1. Metrics of target images and predicted images and their deviation.

No.	Metrics	Target	Predicted	Deviation
Sample 1	CPP	94.4899	94.0496	0.4403
	MPC	11.4896	11.0152	0.4744
	EME	30.5660	28.4836	2.0824
	IC	9.7094	9.7622	−0.0528
	Entropy	7.6945	7.6157	0.0788
Sample 2	CPP	165.5337	164.0485	1.4852
	MPC	18.3142	17.6326	0.6816
	EME	45.7666	31.6619	14.1047
	IC	10.1010	9.9180	0.1830
	Entropy	7.7262	7.6916	0.0346
Sample 3	CPP	136.7770	133.6527	3.1234
	MPC	15.6801	15.1603	0.5198
	EME	39.3058	34.6533	4.6526
	IC	9.2267	9.1819	0.0448
	Entropy	7.6764	7.6628	0.0139
Sample 4	CPP	88.2410	85.3299	2.9111
	MPC	6.8062	6.4638	0.3424
	EME	26.6753	27.6096	−0.9343
	IC	8.5703	8.8449	−0.2746
	Entropy	7.1067	7.0160	0.0907

Figure 4 shows the input images and enhanced images of our method and other algorithms. We selected four representative images for a comprehensive comparison, including sequences with multiple targets, no targets, and mixed targets. For the first image, the HE method makes the roof of the car on the road too dark and other parts of the car too bright. Although the SSR [32] and MSR methods do not make the car appear obviously locally too bright or too dark, they make the lines on the road unclear. Our method not only avoids partial over-brightening or over-darkening of the cars, but also maintains the details of the lines on the road. For the second image, the HE method makes the sky darker, resulting in some clouds not being easy to notice. The images processed using the SSR and MSR methods have more clouds, but the details on the road are still unclear. The use of our method to enhance the image can not only clearly exhibit the clouds in the sky, but also preserve the details on the road. For the third image, the HE method makes the car and the building on the right appear too bright, and the SSR and MSR methods make some textures of the building blurred, so their images are not as detailed as those of the HE method. Our method not only avoids the local over-brightness caused by the HE method, but also makes the details of the building clearer than the SSR and MSR methods. For the fourth image, the HE method not only makes the tires of the car appear too bright, but also gives the trees above part of the image similar brightness to the night sky, which lowers the contrast between trees and the night sky. Our proposed method improves the contrast between trees and the night sky and clarifies the details between layers.

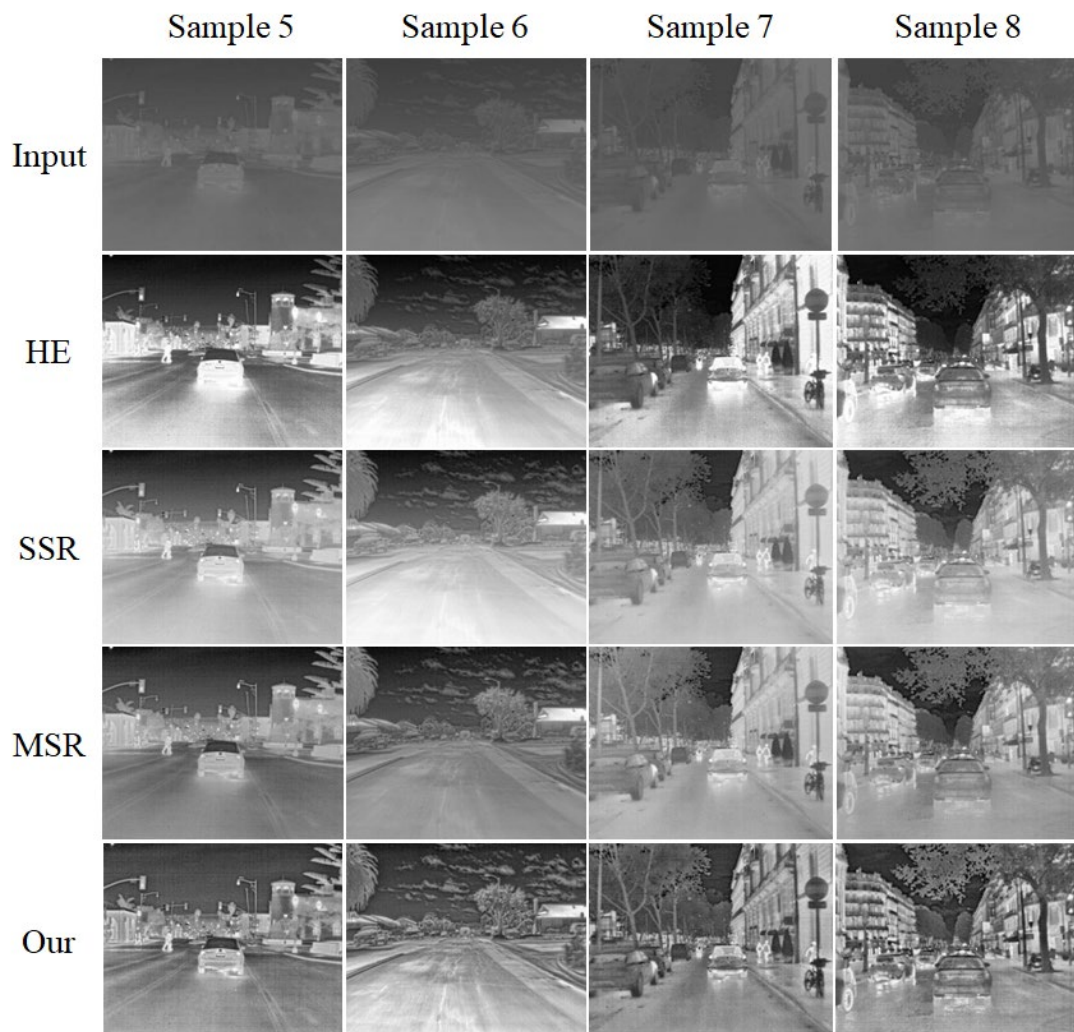


Figure 4. Results of different infrared image enhancement algorithms.

Table 2 shows the objective evaluation index values for sample 5 and sample 6 in Figure 4. We can see in sample 5 that the CPP and MPC values of the image enhanced using the proposed method are larger than those of images enhanced using the other methods. The EME values of the images enhanced using our method are lower than those of images enhanced using the HE method, but higher than those using the SSR and MSR methods. In terms of image sharpness, the IC values of the images enhanced using the proposed method are lower than those of images enhanced using the HE and MSR methods. For sample 6, the CPP and MPC values of the images enhanced using the proposed method are significantly higher than those of images enhanced using the other methods, and the EME values of the enhanced images are also higher than those of images enhanced using the other methods. In terms of image sharpness, the IC values of the images enhanced using the proposed method are lower than those of images enhanced using the HE and MSR methods in samples 6 and 7. In addition, a comparison of the mean values of 300 images in test dataset shows that our designed algorithm has a clear advantage in CPP, MPC, and EME evaluations, but is slightly inferior to MSR in IC comparisons. Therefore, improving IC will be the main direction of the subsequent optimization of our algorithm. The above subjective evaluation and objective index evaluation show that the proposed method can not only enhance the contrast of the infrared image, but also highlight the image details, which can effectively improve the quality of infrared images.

Table 2. Evaluation indexes of different enhancement algorithms.

	Method	CPP	MPC	EME	IC
Sample 5	HE	79.8993	7.2304	27.0587	10.6582
	SSR	53.3885	3.2250	15.6223	7.0078
	MSR	59.1110	4.3980	19.9183	12.7831
	Our	87.1325	7.3228	23.2544	10.3215
Sample 6	HE	48.5970	3.0053	20.9383	11.5948
	SSR	48.2287	2.6711	15.2022	8.4336
	MSR	55.2908	3.6576	12.1363	13.5185
	Our	89.7028	7.0560	26.1675	10.1935
Average	HE	60.9128	5.0932	22.0208	9.5812
	SSR	45.2971	2.9945	13.4705	8.1280
	MSR	60.6530	2.0377	18.2294	10.2501
	Our	82.8761	7.2801	26.8362	9.7684

To study the computational speed of different algorithms, 10 images of size 200×200 were tested using an i5 CPU. Table 3 shows the average time required for enhancing the ten images using MSR, LEPF [18], PSO [33], and the proposed method. The convolutional neural network method proposed in this study requires the shortest average time of 2.02 s, and the MSR algorithm is the next shortest. In contrast, the LEPF algorithm takes the longest average time of 302.3 s. This shows the unique advantage of the short time required for the convolutional neural network method to enhance the image.

Table 3. Average time required for infrared enhancement using different algorithms.

Method	Average Time (s)
MSR	2.18
PSO	4.03
LEPF	302.3
our	2.02

6. Summary

In this paper, a convolutional neural network model for low-contrast infrared grayscale image enhancement is proposed, which directly learns the mapping relationship between low-contrast images and high-contrast images. Low- and high-contrast images are considered the input and output of the model for training. To overcome the lack of a large amount of training data, the brightness and clarity of the infrared images are randomly reduced to form sample pairs. Experiments on the training and test sets demonstrate the advantages of our method over other methods, including its advantages in enhancing the quality of infrared images as well as in processing speed. The proposed algorithm serves as a precursor algorithm for automatic driving image recognition, which not only greatly improves the image processing speed, but also enhances the contrast between the target and the background. In addition, the algorithm can also be used for image enhancement processing in complex tracking systems, which can quickly and effectively deal with the noise in infrared images and improve the contrast of images.

Author Contributions: Conceptualization, F.Z.; methodology, L.F.; software, L.F.; validation, L.F.; formal analysis, S.Z.; investigation, S.Z.; resources, S.Z.; data curation, S.Z.; writing—original draft preparation, S.Z.; writing—review and editing, F.Z.; visualization, L.F.; supervision, F.Z.; project administration, F.Z.; funding acquisition, F.Z. All authors have read and agreed to the published version of the manuscript.

Funding: This research received no external funding.

Institutional Review Board Statement: Not applicable.

Informed Consent Statement: Not applicable.

Data Availability Statement: Restrictions apply to the availability of these data. Data was obtained from Thinkmore company and are available from the authors with the permission of Thinkmore company.

Conflicts of Interest: The authors declare no conflict of interest.

References

1. Ju, J.; Zheng, H.; Li, C.; Li, X.; Liu, H.; Liu, T. AGCNNs: Attention-guided convolutional neural networks for infrared head pose estimation in assisted driving system. *Infrared Phys. Technol.* **2022**, *123*, 104146. [\[CrossRef\]](#)
2. Jia, Y.; Wang, H.; Chen, W.; Wang, Y.; Yang, B. An attention-based cascade R-CNN model for sternum fracture detection in X-ray images. *CAAI Trans. Intell. Technol.* **2022**, *7*, 658–670. [\[CrossRef\]](#)
3. Zhang, Q.; Xiao, J.; Tian, C.; Lin, J.C.; Zhang, S. A robust deformed convolutional neural network (CNN) for image denoising. *CAAI Trans. Intell. Technol.* **2022**, *8*, 331–342. [\[CrossRef\]](#)
4. Dai, D.; Li, Y.; Wang, Y.; Bao, H.; Wang, G. Rethinking the image feature biases exhibited by deep convolutional neural network models in image recognition. *CAAI Trans. Intell. Technol.* **2022**, *7*, 721–731. [\[CrossRef\]](#)
5. Zhao, C.; Wang, J.; Su, N.; Yan, Y.; Xing, X. Low contrast infrared target detection method based on residual thermal backbone network and weighting loss function. *Remote Sens.* **2022**, *14*, 177. [\[CrossRef\]](#)
6. Guoqiang, W.; Hongxia, Z.; Zhiwei, G.; Wei, S.; Dagong, J. Bilateral filter denoising of Lidar point cloud data in automatic driving scene. *Infrared Phys. Technol.* **2023**, *131*, 104724. [\[CrossRef\]](#)
7. Yang, Z.L. Intelligent Recognition of Traffic Signs Based on Improved YOLO v3 Algorithm. *Mob. Inf. Syst.* **2022**, *2022*, 7877032. [\[CrossRef\]](#)
8. Ren, B.; Cui, J.Y.; Li, G. A Three-dimensional Point Cloud Denoising Method Based on Adaptive Threshold. *Acta Photonica Sin.* **2022**, *51*, 319–332.
9. Li, Y.; Zhang, Y.; Geng, A.; Cao, L.; Chen, J. Infrared image enhancement based on atmospheric scattering model and histogram equalization. *Opt. Laser Technol.* **2016**, *83*, 99–107. [\[CrossRef\]](#)
10. Li, S.; Jin, W.; Li, L.; Li, Y. An improved contrast enhancement algorithm for infrared images based on adaptive double plateaus histogram equalization. *Infrared Phys. Technol.* **2018**, *90*, 164–174. [\[CrossRef\]](#)
11. Liu, X.; Pedersen, M.; Wang, R. Survey of natural image enhancement techniques: Classification, evaluation, challenges, and perspectives. *Digit. Signal Process.* **2022**, *127*, 103547. [\[CrossRef\]](#)
12. Singh, K.K.; Pandey, R.K.; Suman, S. Contrast enhancement using lifting wavelet transform. In Proceedings of the 2014 International Conference on Control, Instrumentation, Communication and Computational Technologies (ICCICCT), Kanyakumari District, Kanyakumari, India, 10–11 July 2014; Volume 33, pp. 446–471.
13. Zhang, F.; Xie, W.; Ma, G.; Qin, Q. High dynamic range compression and detail enhancement of infrared images in the gradient domain. *Infrared Phys. Technol.* **2014**, *67*, 441–454. [\[CrossRef\]](#)
14. Song, Q.; Wang, Y.; Bai, K. High dynamic range infrared images detail enhancement based on local edge preserving filter. *Infrared Phys. Technol.* **2016**, *77*, 464–473. [\[CrossRef\]](#)
15. Zhou, Z.; Shi, Z.; Ren, W. Linear Contrast Enhancement Network for Low-Illumination Image Enhancement. *IEEE Trans. Instrum. Meas.* **2022**, *72*, 1–16. [\[CrossRef\]](#)
16. Bi, X.; Shang, Y.; Liu, B.; Xiao, B.; Li, W.; Gao, X. A Versatile Detection Method for Various Contrast Enhancement Manipulations. *IEEE Trans. Circuits Syst. Video Technol.* **2023**, *33*, 491–504. [\[CrossRef\]](#)
17. Zhu, X.; Lin, M.; Zhao, M.; Fan, W.; Dai, C. Adaptive underwater image enhancement based on color compensation and fusion. *Signal Image Video Process.* **2023**, *17*, 2201–2210. [\[CrossRef\]](#)
18. Pang, L.; Zhou, J.; Zhang, W. Underwater image enhancement via variable contrast and saturation enhancement model. *Multimedia Tools Appl.* **2023**, 1–22. [\[CrossRef\]](#)
19. Shen, L.; Yue, Z.; Feng, F.; Chen, Q.; Liu, S.; Ma, J. Msr-net: Low-light image enhancement using deep convolutional network. *arXiv* **2017**, arXiv:1711.02488.
20. Kuang, X.; Sui, X.; Liu, Y.; Chen, Q.; Gu, G. Single infrared image enhancement using a deep convolutional neural network. *Neurocomputing* **2018**, *332*, 119–128. [\[CrossRef\]](#)
21. Cai, B.; Xu, X.; Jia, K.; Qing, C.; Tao, D. DehazeNet: An End-to-End System for Single Image Haze Removal. *IEEE Trans. Image Process.* **2016**, *25*, 5187–5198. [\[CrossRef\]](#)
22. Qian, Y.; Jiang, Z.; He, Y.; Zhang, S.; Jiang, S. Multi-scale error feedback network for low-light image enhancement. *Neural Comput. Appl.* **2022**, *34*, 21301–21317. [\[CrossRef\]](#)
23. Wang, D.; Lai, R.; Guan, J. Target attention deep neural network for infrared image enhancement. *Infrared Phys. Technol.* **2021**, *115*, 103690. [\[CrossRef\]](#)
24. Jia, X.; Zhu, C.; Li, M.; Tang, W.; Zhou, W. LLVIP: A visible-infrared paired dataset for low-light vision. In Proceedings of the IEEE/CVF International Conference on Computer Vision, Montreal, BC, Canada, 11–17 October 2021; pp. 3496–3504.
25. Bao, C.; Cao, J.; Hao, Q.; Cheng, Y.; Ning, Y.; Zhao, T. Dual-YOLO Architecture from Infrared and Visible Images for Object Detection. *Sensors* **2023**, *23*, 2934. [\[CrossRef\]](#)

26. Chen, C.-Y.; Chuang, C.-H.; Lin, H.-Y.; Zhuo, D.-Y. Imaging evaluation of computer-generated hologram by using three-dimensional modified structural similarity index. *J. Opt.* **2022**, *24*, 055702. [[CrossRef](#)]
27. Kim, B.; Ryu, K.H.; Heo, S. Mean squared error criterion for model-based design of experiments with subset selection. *Comput. Chem. Eng.* **2022**, *159*, 107667. [[CrossRef](#)]
28. Luque-Chang, A.; Cuevas, E.; Pérez-Cisneros, M.; Fausto, F.; Valdivia-González, A.; Sarkar, R. Moth Swarm Algorithm for Image Contrast Enhancement. *Knowledge-Based Syst.* **2020**, *212*, 106607. [[CrossRef](#)]
29. Park, P.C.; Choi, G.W.; Zaid, M.M.; Elganainy, D.; Smani, D.A.; Tomich, J.; Samaniego, R.; Ma, J.; Tamm, E.P.; Beddar, S.; et al. Enhancement pattern mapping technique for improving contrast-to-noise ratios and detectability of hepatobiliary tumors on multiphase computed tomography. *Med Phys.* **2019**, *47*, 64–74. [[CrossRef](#)]
30. Shin, Y.-G.; Park, S.; Yeo, Y.-J.; Yoo, M.-J.; Ko, S.-J. Unsupervised Deep Contrast Enhancement With Power Constraint for OLED Displays. *IEEE Trans. Image Process.* **2019**, *29*, 2834–2844. [[CrossRef](#)]
31. Li, M.; Ruan, B.; Yuan, C.; Song, Z.; Dai, C.; Fu, B.; Qiu, J. Intelligent system for predicting breast tumors using machine learning. *J. Intell. Fuzzy Syst.* **2020**, *39*, 4813–4822. [[CrossRef](#)]
32. Xie, S.J.; Lu, Y.; Yoon, S.; Yang, J.; Park, D.S. Intensity Variation Normalization for Finger Vein Recognition Using Guided Filter Based Single Scale Retinex. *Sensors* **2015**, *15*, 17089–17105. [[CrossRef](#)]
33. Wan, M.; Gu, G.; Qian, W.; Ren, K.; Chen, Q.; Maldague, X. Particle swarm optimization-based local entropy weighted histogram equalization for infrared image enhancement. *Infrared Phys. Technol.* **2018**, *91*, 164–181. [[CrossRef](#)]

Disclaimer/Publisher’s Note: The statements, opinions and data contained in all publications are solely those of the individual author(s) and contributor(s) and not of MDPI and/or the editor(s). MDPI and/or the editor(s) disclaim responsibility for any injury to people or property resulting from any ideas, methods, instructions or products referred to in the content.